Design and Manufacturing of an HTS Helical Undulator Demonstrator for Compact FELs

S. C. Richter, A. Ballarino, A. Bernhard, and A.-S. Müller

(Invited Paper)

***Abstract*—Among all superconducting undulator geometries, a helical undulator provides a very compact geometry and further is more effective in producing synchrotron radiation, providing circularly polarized photons, which are widely usable for synchrotron radiation users. These characteristics make it a very attractive option for realizing more compact free-electron lasers, requiring a combination of short-period and high-field undulators to produce coherent light up to X-rays. To further increase the magnetic field at 4.2 K and achieve larger operating margins as compared with low-temperature superconductors, the application of a high-temperature superconductor (HTS) in the form of coated rare-Earth barium copper oxide tapes was investigated. This article presents the design and manufacturing work done on an HTS helical undulator prototype—the very first helical undulator design based on HTS tape winding to the best of the authors' knowledge. To provide proof of concept, a five-period short-model demonstrator was realized by a bifilar, no-insulation winding scheme from a single piece of HTS cable, wound with a period length of 13 mm and a magnetic gap of 5 mm. First powering tests at 77 K, performed in liquid nitrogen, revealed stable operations up to the calculated critical current of 140 A and even above. Higher currents of up to 160 A showed the expected coil protection, enabling the current to bypass the appearance of normal conducting zones and redistribute without degrading the superconductor.**

***Index Terms*—Free-electron lasers (FELs), high-temperature superconductors (HTS), superconducting devices, undulators.**

I. Introduction

PRESENT and future compact light sources aim for photon production up to the hard X-ray energy spectrum with high brilliance. Consequently, short-period high-field undulators become necessary for photon production as more compact machines, such as a free-electron laser (FEL), commonly operate at lower energies. This was recently investigated by the CompactLight project (XLS), funded by the European Commission, with 13 mm period undulators and electron beam energies in the range of 2.5–5.5 GeV [1].

Superconducting undulators represent state-of-the-art technology for high fields and are currently built using low-temperature superconductors, commonly Niobium–titanium (Nb-Ti). Examples of successfully operating Nb-Ti insertion devices can be found at the synchrotrons KARA, located at the Karlsruhe Institute of Technology (KIT), APS, Argonne National Laboratory, and lately also at ANSTO [2], [3], [4], [5].

Driven by the goal to generate higher magnetic flux density amplitudes for the parameter space of short-period undulators, we investigate the application of commercially available high-temperature superconductors (HTS) to undulator magnets, i.e., HTS in the form of coated rare-Earth barium copper oxide (*Re*BCO) superconducting tapes. The HTS *Re*BCO has the characteristics of behaving superconducting up to 90 K plus having a high upper critical field ($B_{c2}(4\,\mathrm{K}) \approx 100\,\mathrm{T}$) at low temperatures [6], [7]. Both make it an up-and-coming material for future superconducting undulators and accelerator magnets by relaxing cryogenic requirements and also improving magnets' performances. In this context, particularly relaxed cryogenic requirements or operation at higher temperatures, thus implying lower cooling power consumption, may lower the operational cost owing to an improved Carnot efficiency [8], [9]. Consequently, the application of *Re*BCO may be interesting for reducing the overall ecological footprint of light sources and their superconducting devices. The potential of applying *Re*BCO to superconducting undulators to enlarge the accessible parameter space in terms of the undulator period length λ_u, the magnetic gap, and the magnetic flux density B was already demonstrated in previous work [10], [11], [12]. Here, especially undulator period lengths of $\lambda_u \leq 20\,\mathrm{mm}$ may profit, due to the high current densities in small volumes. Operating HTS for generating high magnetic flux density commonly comes with rather high operating current densities, which makes the superconducting coil challenging to protect. In the following, this issue is treated by using a no-insulation (NI) approach with rather large copper terminals, which should make the magnet self-protected.

This concept was recently demonstrated for HTS undulator vertical racetrack (VR) prototype coils, reaching safe operation up to engineering current densities J_e of 2.3 kA/mm^2 at 4.2 K for $\lambda_u = 13\,\mathrm{mm}$ [13]. Safe operations even 10% beyond the critical

Manuscript received 25 September 2023; revised 27 November 2023; accepted 2 January 2024. Date of publication 22 January 2024; date of current version 13 February 2024. This work was supported by the Wolfgang Gentner Program of the German Federal Ministry of Education and Research. *(Corresponding author: S. C. Richter.)*

S. C. Richter was with CERN, 1211 Geneva, Switzerland, and also with the Karlsruhe Institute of Technology (KIT), 76131 Karlsruhe, Germany. He is now with Paul Scherrer Institute (PSI), 5232 Villigen, Switzerland (e-mail: sebastian.richter@psi.ch).

A. Ballarino is with CERN, 1211 Geneva 23, Switzerland.

A. Bernhard and A.-S. Müller are with the Karlsruhe Institute of Technology (KIT), 76131 Karlsruhe, Germany.

Color versions of one or more figures in this article are available at https://doi.org/10.1109/TASC.2024.3356449.

Digital Object Identifier 10.1109/TASC.2024.3356449

current were presented in this study. The application of NI and partially insulated wound HTS undulator coils was also proven in other experimental studies, e.g., in a jointless VR winding scheme for $\lambda_u = 16\,\text{mm}$ with $J_e(4.2\,\text{K})$ of $2.1\,\text{kA/mm}^2$ [14]. Here, protection was challenging to realize in case of a quench. This also holds for NI stacked laser-structured *Re*BCO superconducting tapes for $\lambda_u = 8\,\text{mm}$ [15], [16]. Other compact HTS undulator concepts, such as magnetized bulk staggered arrays showed promising performances but had to cope with flux creep over time [17], [18].

In this article, we summarize the work done in a collaboration between CERN and KIT on the very first HTS helical undulator (H^2U) design, the H^2U, based on wound *Re*BCO tape and its demonstrator magnet with $\lambda_u = 13\,\text{mm}$ and a 5 mm gap.

A five-period short-model demonstrator magnet was successfully built and tested with first powering tests at 77 K, demonstrating the proof of concept. Stable operations up to the measured critical current and beyond demonstrated the working design including the protection and are discussed in the following.

II. H^2U Coil Design

The presented H^2U design is based on a bifilar helix, to be wound with HTS *Re*BCO tape. A five-period short model was realized in the first step as a demonstrator magnet with only 12 turns, representing 10% of the totally needed 120 turns to fill the groove. These innermost turns form the most critical region of the design with respect to the background magnetic field and bending radius, as presented in the following sections. As the utilization of HTS increases the risk of a quench due to the high operating current densities at low temperatures ($J_e(4.2\,\text{K}) \geq 2\,\text{kA/mm}^2$), a dry and NI winding approach with *Re*BCO tape as superconductor was chosen to deal with this issue. In the scenario of an emerging normal conducting zone, the current has the option to redistribute among the turns, thus within the tape stack, which either enlarges the critical zone or reduces the effective current in the normal zone, both may lower the hotspot temperature. Consequently, this should make the magnet self-protected, delay the heat-up, and/or bypass the current completely thus avoiding a quench.

The current flows in opposing directions within the two superconducting helical tape stacks, forming the bifilar structure and thus creating the helical on-axis magnetic field. Consequently, the winding body displayed in Fig. 1 must work as an insulator for the two helices. Then, again, in the area of the return spools with copper terminals the current always has the possibility to bypass the helical coil completely by skipping turns and flowing transversely. Therefore, this unique design allows the simultaneous current flow in the superconducting coil and/or a current overflow in the transverse direction in case of an arising voltage over the coil. Earlier performed 2-D electromagnetic parameter space investigations and a projected use case in XLS defined the major design parameters [1]. Here, the winding pitch p of the superconductor is equivalent to the undulator period length λ_u and was set to 13 mm. The magnetic gap of $g = 5\,\text{mm}$ was deduced from the *Re*BCO tape's winding or rather bending

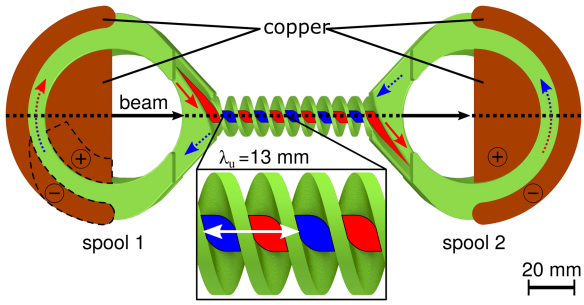

Fig. 1. H^2U design resting on a bifilar helix to be wound with coated *Re*BCO tape. Copper terminals guide the current (colored arrows) in and out as the superconducting tape returns via two spools, following a half spiral to overcome the level difference. The dashed copper parts were realized for the five-period demonstrator magnet.

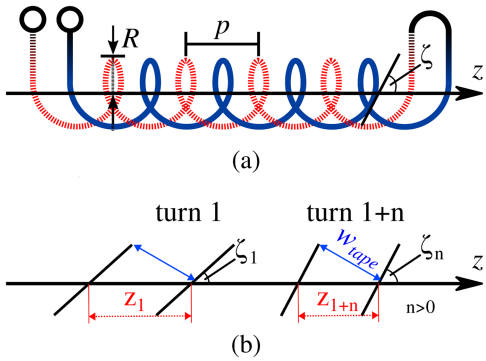

Fig. 2. (a) Schematic bifilar helical structure around the beam axis z with radius $R \equiv g$, the magnetic gap, the pitch $p \equiv \lambda_u$, the undulator period, and the escaping arc ζ. (b) Schematic of the escaping arc ζ and its influence on the tape cross-section along the beam axis z. $\zeta_1 < \zeta_n$ and $z_1 > z_{n+1}$, for $n > 0$.

TABLE I
Design Parameters of the Investigated Helical Undulator Coils, Both to Be Wound With an NI Double Tape Cable

$\lambda_u = 13\,\text{mm}$	**Short Model**	**Demonstrator**
Coil cross-section	$4\,\text{mm} \times 6\,\text{mm}$	$4\,\text{mm} \times 0.6\,\text{mm}$
HTS tape thickness	$50\,\mu\text{m}$	
Substrate	$30\,\mu\text{m}$	
Stabilizer	$15\,\mu\text{m}$	
Number of turns	120	12
J_e in self-field at 77 K (LN_2)		
$J_e(0.25\,\text{T}, 77\,\text{K})$	$320\,\text{A/mm}^2$	$350\,\text{A/mm}^2$
$I_{c,sim}(0.25\,\text{T}, 77\,\text{K})$	128 A	140 A
$B_0(I_c, g = 5\,\text{mm})$	0.14 T	0.1 T
J_e in self-field at 4.2 K (LHe)		
$J_{e,op}(5.5\,\text{T}, 4.2\,\text{K})$	$2000\,\text{A/mm}^2$	-
$I_{sim}(5.5\,\text{T}, 4.2\,\text{K})$	800 A	-
$B_0(I, g = 5\,\text{mm})$	2.0 T	-

radius R and thus was defined by the lowest achievable bending radius of the utilized *Re*BCO tape [19]. Here, a commercially available 4 mm wide HTS tape with one of the smallest bending radii feasible was chosen, thus with a substrate thickness of 30 µm. All significant parameters are sketched in Fig. 2(a) and summarized in Table I. Pitch and winding radius further define

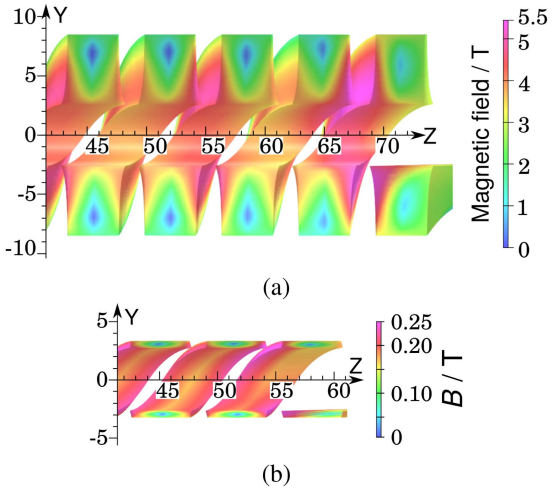

Fig. 3. Cross-sectional view along the beam axis (scale in mm) with the magnetic field B on the tape stacks shown as a contour for (a) the H^{2}U short model with $J_{e,op}(4.2\,\mathrm{K}) = 2\,\mathrm{kA/mm^2}$, and (b) the H^{2}U demonstrator with $J_c(77\,\mathrm{K}) = 350\,\mathrm{A/mm^2}$, both reproduced from [23]. The maximum B appears at the rims, the minimum close to the center of the tape stack.

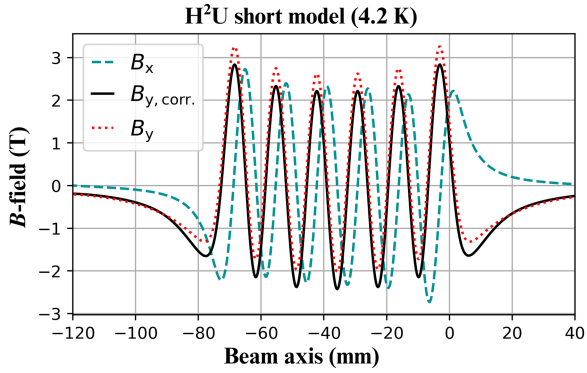

Fig. 4. Magnetic field components and possible correction in $\hat{y}$ along the beam axis $\hat{z}$ of the H^{2}U short model for $J_{e,op}(4.2\,\mathrm{K}) = 2\,\mathrm{kA/mm^2}$. Reproduced from [23].

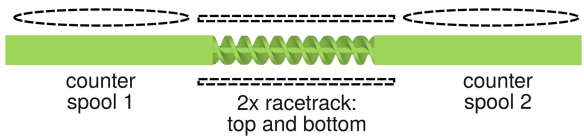

Fig. 5. Side view sketch of a possible correction scheme (dashed) for the H^{2}U short model (cf., Fig. 1) with two mandatory counter solenoids above each spool and two optional racetracks creating a dipolar field over the length of the helical section. However, the latter may influence the HTS coil's J_c .

the so-called escaping arc $\zeta = \arctan(p/2\pi R)$, describing the angle between the beam axis ($\hat{z}$) and the helical winding slope. Consequently, the nonrectangular tape stack cross-section originates from keeping a constant p in ζ and varying R with every turn as sketched in Fig. 2(b) and in Fig. 7(a).

A. 3-D Electromagnetic Modeling

Opera was used to perform 2-D and 3-D electromagnetic calculations [20], which were based on a worst-case scenario: the absolute magnetic field was considered perpendicular to the *Re*BCO's plane. Spot checks at 4.2 K supported this assumption where greater than 99% of the absolute field on the superconductor was given by the perpendicular field component. The used *Re*BCO tape was characterized with a critical current surface based on a database and combined with fits done at CERN [21], [22].

The H^{2}U was investigated for two scenarios: First, as a short model with a focus on operation with high magnetic fields and forces at 4.2 K, and second, as a short demonstrator with a focus on the proof of concept and the critical current limit at 77 K. Contour plots of the calculated fields on the conductor are displayed in Fig. 3. An engineering current density of $J_{e,op}(4.2\,\mathrm{K}, 5.5\,\mathrm{T}) = 2\,\mathrm{kA/mm^2}$ was found for the short model H^{2}U to ensure safe operation with a rather conservative safety margin of around 20% to the critical current density J_c. The demonstrator magnet was calculated with a $J_c(77\,\mathrm{K}, 0.25\,\mathrm{T}) = 350\,\mathrm{A/mm^2}$. A summary of the electromagnetic calculations can be found in Table I.

The on-axis helical magnetic field is described by the components B_x and B_y. Fig. 4 shows both components along the short model's beam axis with their periodical characteristic. However, the two solenoidal-like return spools, may not only cause local field disruptions but also globally shift the B_y-component due to the v-shape tape stack endings. The first can be corrected rather simply with additional external solenoids, the latter may be corrected in the first order with two racetrack coils, creating a 0.38 T dipole field along the bifilar helix, if pure circular polarization is needed. In other respects, here, no correction in B_y would cause elliptical polarization, which is also of interest. These possible, first-order correction coils are sketched in Fig. 5. Further investigations are needed to improve this correction, which might alternatively include tilting or moving the return spools further away from the beam axis. A parallel exit of the tape stacks instead of the v-shape might be also a very interesting option that would significantly lower the need for these corrections or make them even redundant [23].

B. Mechanical Modeling

ANSYS was used to perform mechanical strain and stress calculations for the H^{2}U short model [24]. This analysis focused on the bifilar helix of the magnet as it is the most crucial in generating the undulator field, thus material deformations may cause field variations. A cool-down from 300 to 4.2 K was considered and superimposed with the appearing Lorentz forces during powering in the high operating current regime, analyzed above for $J_{e,op}(4.2\,\mathrm{K}, 5.5\,\mathrm{T})$. Element force densities were used to link the Opera 3-D results to the mechanical ANSYS model.

Calculations showed that the symmetric geometry of the bifilar helix distributes the Lorentz forces rather equally over the conductor packs giving maxima in the order of 200 N or rather 4 MPa over a quarter section, as seen in Fig. 6(a). For the cool-down analysis, the helical coil was described by its composing materials and their volume percentage, i.e., the 4 mm

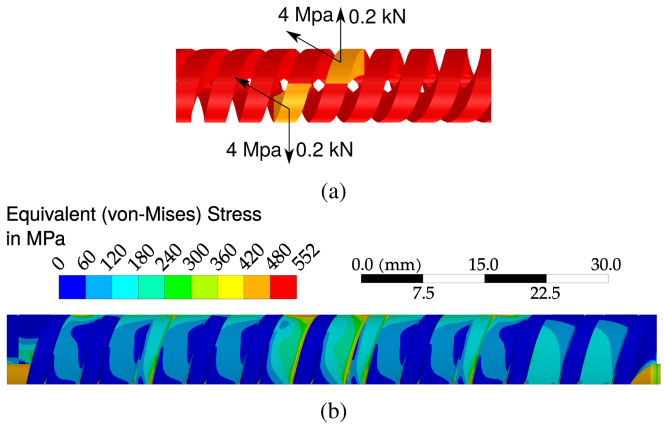

Fig. 6. Quarter sections of the H^{2}U mechanically investigated for $J_{e,op}(4.2\,\mathrm{K}) = 2\,\mathrm{kA/mm^2}$. (a) Lorentz forces. (b) Equivalent stress caused by the combination of cool-down to 4.2 K and subsequent powering. Reproduced from [23].

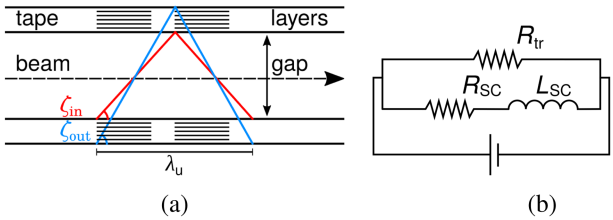

Fig. 7. (a) Constant pitch (λ_u) for layer-by-layer winding can only be achieved by a variation of the winding angle, thus $\zeta_{out} > \zeta_{in}$, resulting in a fan of layers exiting the helix. (b) Simplified circuit diagram of the NI H^{2}U magnet with superconductive and transverse (tr) current paths.

wide HTS tape was simplified conservatively as a homogeneous material based on thicknesses of 3 µm YBCO, 7 µm silver, 100 µm stainless steel, and 40 µm copper. The winding body was modeled using solid stainless steel for the H^{2}U short model. Connections between the tape stack and the winding former were defined as bonded to calculate the maximum possible stress, accepting the risk of overestimating the stress. As a result, an impact of the cool-down was found with single high-stress regions going up to 552 MPa, and thus staying below threshold values in the region of 600 MPa [25]. The relative high stress might be of concern, as it may damage the superconducting *Re*BCO layer. Therefore, although this analysis is rather conservative, future test windings should include experimental analysis, e.g., by using pressure measurement films in between the tape layers. In addition, further materials for the winding body, such as titanium, should be investigated aiming to lower the maximum stress on the conductor.

C. Heat Load Estimation

When designing a superconducting undulator magnet, the heat load must always be taken care of as local heating will decrease the HTS performance and may even cause a quench. In our presented H^{2}U design, the vacuum chamber is foreseen to be inserted with a surrounding 0.5 mm distance to the HTS coil, allowing for thin insulation. When scaling up the H^{2}U short model to a full-size magnet, 2 W/m was agreed to be a practical value for the cooling power during usual operation adapted from experiences gained at KARA, KIT [26]. This directly implies a limit of $13\,\mathrm{mm} \cdot 2\,\mathrm{W/m} = 26\,\mathrm{mW}$ per period.

Electrical joints are the major contributor of heat loads for superconducting undulators. As the design foresees winding the H^{2}U from one or two pieces of HTS tape, the half-circular copper current leads with radius $R_{spool} = 35$ mm will be the only joints to take into account. Here, the scenario with a two-tape stack cable is considered for a larger estimate. With the inner curved area of $A_{joint} = 4\,\mathrm{mm} \cdot 2\pi \cdot 35\,\mathrm{mm} \approx 8.8\,\mathrm{cm^2}$. Further, a configuration of both HTS tapes face-to-back (f2b) was considered, keeping the *Re*BCO layer always under compression, thus facing the winding body, for achieving the smallest bending radius and providing direct contact to *Re*BCO layer from the inner copper [face-to-face (f2f)]. Joint area resistances of $R_{f2b} = 290\,\mathrm{n\Omega cm^2}$ and $R_{f2f} = 36\,\mathrm{n\Omega cm^2}$ were demonstrated in experimental studies [27], yielding

$$\begin{aligned} P &= 2\,(P_1 + P_2) \\ &= 2\left(I_{op}(4.2\,\mathrm{K})^2 \cdot \frac{R_{f2f}}{A_{joint}} + \left(\frac{I_{op}(4.2\,\mathrm{K})}{2}\right)^2 \cdot \frac{R_{f2b}}{A_{joint}}\right) \\ &\approx 16\,\mathrm{mW}\,. \end{aligned} \tag{1}$$

This value is well below the threshold for the five investigated periods but will stay constant also for more periods, as the return spools stay the same. As the heat load is mainly expected on the two return spools, a local increase of cooling power would be well feasible, also regarding the copper high-current leads.

III. Coil Manufacturing and Experimental Setup

The H^{2}U demonstrator was manufactured as a NI coil, winding one continuous 4 mm wide and 100 µm thick two-tape stack HTS cable onto the helical winding body. Polyamide 11 with 25% glass fiber (GF) was used as material to create the winding body by means of additive manufacturing. The material choice was motivated to be a more lightweight approach that combined the needed rigidity and insulation for this very first demonstrator test at 77 K, compared with the foreseen material stainless steel or further alternatives, such as aluminum or titanium. Oxygen-free copper blocks were used as current in- and outlets. Their size was roughly a fifth of the H^{2}U short model's design, however, this demonstrator was designed for operation at 77 K only with a limited operational current.

Starting the coil winding, both the cable's HTS tapes were soldered to the inner copper terminal, one attached to the other, using Sn62Pb36Ag2 for less than 2 *min* at 180 °C. Afterward, the two tapes were dry-wound simultaneously with a controlled winding tension of 5.5 N for each tape until the goal of 12 layers was reached. Here, the introduced escaping arc ζ [cf., Fig. 2(a)] was of high importance as it defined the winding angle, therefore a smooth fit of the tape into the 4.2 mm wide winding groove. The variation of ζ had to be taken into account with every turn, as it depends on the winding diameter as sketched in Fig. 7(a). A total amount of seven voltage taps (Vtaps) were clamped

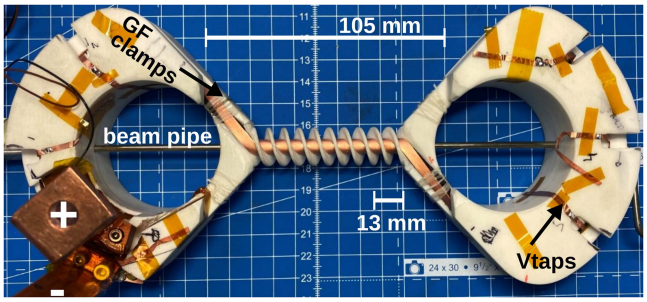

Fig. 8. H^2U demonstrator with attached Vtaps. As support, only glass fiber (GF) clamps were used in critical regions, and a dummy beam pipe.

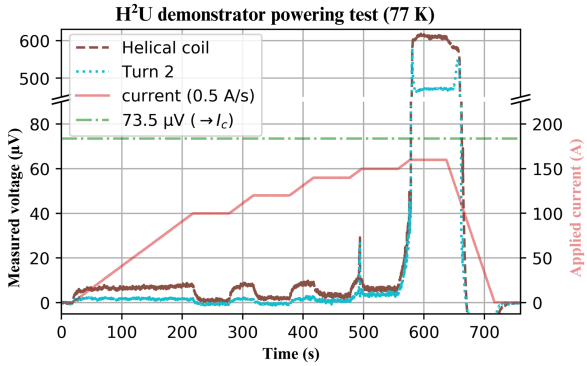

Fig. 9. Measured voltage responses over the H^2U demonstrator for a powering test with current plateaus at 77 K. A clear increase in voltage was detected after having reached I_c.

in between every turn as instrumentation to track the voltage across the coil. The coil was closed by soldering the outer copper terminal to the last turn and adding an additional bridge splice of the same cable from the last turn to the outfacing copper side. The same soldering procedure as for the innermost turn was used. As the coil was wound without insulation layers in between turns, the current always can freely redistribute within the coil in case of facing any resistance, as seen in Fig. 7(b). The superconducting current path of the helical coil is described as an inductive resistor when the operation is started below the critical temperature in stable conditions while skipping single turns or the entire coil transversely involves an ohmic resistance, depending on the turn-to-turn resistance.

Overall, the tape stack had a smooth fit on the winding body. During winding tests, minor gaps were noticed in the regions between the helix and the return spool. Clamps during and after the winding process improved these regions. The use of spacers made of copper may further optimize these regions if necessary. Fig. 8 shows the H^2U demonstrator after winding with current leads clamped to the copper terminals.

IV. Experimental Results and Discussion

As introduced above, the innermost turns of the H^2U design see not only the smallest bending radii from 2.5 mm upward but also partly the highest fields, and the greatest variation in the winding angle. Consequently, the H^2U demonstrator realizes the most demanding parts and can be seen as the first proof of concept for the entire design. However, the first simplified copper current leads were designed for maximum currents of around 200 A, focusing on first powering tests at 77 K rather than lower temperatures and higher currents. These first tests were performed in a liquid nitrogen (LN_2) bath. To ensure the integrity of the measured data, various electrical powering test runs and thermal cycles were executed. A quench detector was active with a threshold of 1 mV to cut the current if needed while the data acquisition ran with a 5 Hz sample rate. The critical current I_c was derived from the electrical field criterion of 1 μV/cm, applied to one turn length of the demonstrator that is about 73.5 cm, thus 73.5 μV. Therefore, the global I_c of the coil is defined by the first turn hitting its local threshold.

After the cool-down to 77 K, the foreseen operation was always checked with current ramps up to 30 A with 0.25 A/s. As seen earlier, the current can redistribute in this NI design, therefore a rise in voltage over the coil is expected when stepping or ramping the current caused by the inductance or the transverse flow. During operation, when all current has settled in the superconductor, the voltage will drop to zero. The investigations presented in the following section demonstrate this behavior. Plots are reproduced from [23].

A. Current Ramping

To investigate the H^2U's performance up to I_c and beyond, the current was ramped with 0.5 A/s to plateaus of 100, 120, 140, 150, and 160 A for 60 s, allowing the voltage to stabilize. This procedure is shown in Fig. 9 with only one single-turn example for legibility. After having reached the first plateaus, the voltage decayed to a stable value staying well below the critical threshold. First voltage spikes in turn 2 and a slight rise in the decayed overall voltage were detected at 150 A, yet, well below the limit. The current is expected to flow to a small extent in the copper matrix when driven further up, until it may bypass the coil transversely causing an elevated voltage plateau. This happened when ramping the current further up to 160 A when the voltage shot over 73.5 μV but stabilized at around 600 μV. As this relatively high voltage plateau could be reproduced in multiple powering test runs, it was interpreted as caused by the transverse current flow through the tape stack in between the copper terminals. Consequently, the H^2U's self-protection provided by its NI coil design was successfully triggered.

As a result, $I_c = 150$ A was found for this H^2U demonstrator, manufactured with a noninsulated two-tape stack cable. This can be seen as in agreement with the above-presented simulations, as they consider the worst-case scenario and end up with about 6.5% less. Driving down the current also let the voltage drop back to zero. After multiple thermal and powering cycles, the coil did not show any degradation in performance, although going multiple times 6% over I_c.

B. Effective Time Constant

With 12 turns, the H^2U demonstrator only consists of 10% of the short model and therefore is expected to be (dis-) charged rather quickly. This can directly be investigated by observing the voltage increase and decrease for a current step function in the superconducting operating regime. From Fig. 7(b), the voltage's

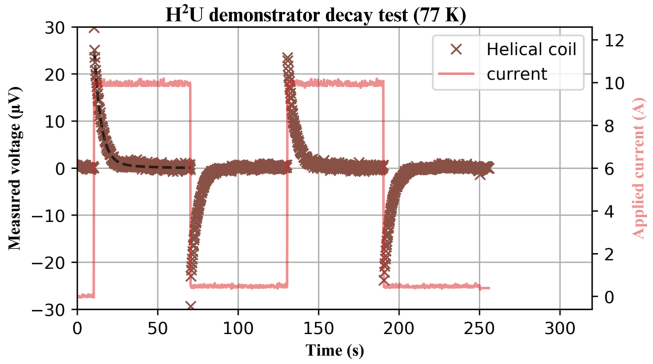

Fig. 10. Measured decaying voltages over the H^2U demonstrator for a 10 A current step function at 77 K. The black dashed line displays an exponential decay fit determining τ.

reaction can be derived as an exponential decay, here simplified with one term only [28]

$$U(t) \approx a \cdot \mathrm{e}^{-t/\tau} \tag{2}$$

where a is a constant and τ is the effective time constant.

To investigate τ, a current step function with plateaus of 10 and 0.5 A was chosen with a dwell of 60 s. The resulting measured voltage responses with their exponential behaviors can be seen in Fig. 10, where the effective time constant was calculated as $\tau \approx 4.7$ s for the 12 superconducting coil turns. Therefore, the magnetic field should be built up after a time of $5 \times \tau$ in this demonstrator magnet.

The scaling to a full-size short model or even a full undulator magnet, yet, might be more complex for multiple reasons: the full design includes 120 turns, where technical factors, such as a stable winding tension play a crucial role, but also the size of the current leads will be increased. In addition, the helical structure, and thus the entire coil, will be much larger for a full-size undulator, changing the inductance significantly.

V. Conclusion

A design study of an H^2U based on NI coated *Re*BCO tape was performed. The presented design with a period length of $\lambda_u = 13$ mm and a 5 mm gap was followed up by the manufacturing of a short model demonstrator magnet, having five periods and 12 turns, corresponding to 10% of the full-groove design. The first powering tests of this H^2U demonstrator at 77 K, in LN_2, showed stable operations up to a critical current of 150 A and thus good agreement with the calculations. going even higher in current, operating values of up to 160 A forced the designed coil protection, an internal current redistribution allowing current to bypass the appearance of normal conducting zones and redistribute without degrading the superconductor. Consequently, a stable coil operation of 6% above the experimentally determined critical current could be demonstrated for over 60 s, providing crucial time for coil protection, e.g., extracting the coil's energy.

In conclusion, the application of coated *Re*BCO superconducting tapes to a helical undulator winding scheme was successfully demonstrated by the H^2U demonstrator for the most critical regions. Stable operation and a working self-protection mechanism at 77 K were presented. The next experimental steps should cover magnetic field measurements along the beam axis at 77 K and potentially be followed with powering tests and measurements at 4.2 K. Here, magnetic field amplitudes in the order of 0.1 T and up to 0.6 T are expected from calculations at the stated temperatures, respectively, demonstrating that operations at higher temperatures are feasible at the cost of a reduction in field amplitude. Then, building and testing a full-stack short-model H^2U would be a logical next step for more detailed studies. Furthermore, the presented HTS undulator makes not only high-current, thus high-field superconducting undulators feasible, but also reduces their dimensions drastically and additionally enables operations at higher temperatures above the commonly used 4.2 K. As a consequence of the latter, a reduction in cooling costs due to relaxed cryogenic requirements may make HTS as materials for undulators an even more attractive choice in the near future.

Acknowledgment

The authors would like to thanks J. Mazet, R. Betemps, and F. Pillon for their support in the manufacturing and design process.

References

[1] G. D'Auria et al., "XLS - D2.3: Conceptual Design Report," Zenedo, 2021. [Online]. Available: www.compactlight.eu
[2] S. Casalbuoni et al., "Superconducting undulators: From development towards a commercial product," *Synchrotron Radiat. News*, vol. 31, no. 3, pp. 24–28, Jun. 2018.
[3] A. Bernhard et al., "A CLIC damping wiggler prototype at ANKA: Commissioning and preparations for a beam dynamics experimental program," in *Proc. Int. Part. Accel. Conf*, Busan, Korea, 2016, pp. 2412–2415.
[4] Y. Ivanyushenkov et al., "Development and operating experience of a 1.1-m-long superconducting undulator at the advanced photon source," *Phys. Rev. Accel. Beams*, vol. 20, no. 10, Oct. 2017, Art. no. 100701.
[5] Superconducting Undulator at ANSTO BioSAXS Beamline produced first light!. Accessed Aug. 2023. [Online]. Available: https://www.noell.bilfinger.com/aktuelles/fachpresse/meldungen-detail/news/superconducting-undulator-at-ansto-biosaxs-beamline-produced-first-light/
[6] A. Golovashkin et al., "Low temperature direct measurements of H_{c2} in HTSC using megagauss magnetic fields," in *Physica C: Supercond.*, vol. 185–189, pp. 1859–1860, 1991.
[7] M. K. Wu et al., "Superconductivity at 93 k. in a new mixed-phase Y-ba-Cu-O compound system at ambient pressure," *Phys. Rev. Lett.*, vol. 58, Mar. 1987, Art. no. 908.
[8] R. Radebaugh, "Cryocoolers: The state of the art and recent developments," *J. Phys.: Condens. Matter*, vol. 21, no. 16, Mar. 2009, Art. no. 164219.
[9] H. J. M. ter Brake and G. F. M. Wiegerinck, "Low-power cryocooler survey," *Cryogenics*, vol. 42, no. 11, pp. 705–718, 2002.
[10] S. C. Richter et al., "High-temperature superconducting undulators for compact free-electron lasers," Talk at the DPG Springmeeting of the section Mater and Cosmos (SMuK), working group accelerator physics, Munich, 2019.
[11] F. Nguyen et al., "XLS - D5.1: Technologies for the CompactLight Undulator," on Zenedo, 2019. [Online]. Available: www.compactlight.eu
[12] S. C. Richter, A. Ballarino, D. Schoerling, T. H. Nes, A. Bernhard, and A. -S. Müller, "Progress on HTS undulator prototype coils for compact FEL designs," *IEEE Trans. Appl. Supercond.*, vol. 32, no. 4, Jun. 2022, Art. no. 4100305.

[13] S. C. Richter, A. Ballarino, A. Bernhard, A. W. Grau, D. S. de Jauregui, and A. -S. Müller, "High-temperature superconducting undulator prototype coils for compact free-electron lasers," *IEEE Trans. Appl. Supercond.*, vol. 33, no. 5, Aug. 2023, Art. no. 4100207.

[14] I. Kesgin, M. Kasa, Y. Ivanyushenkov, and U. Welp, "High-temperature superconducting undulator magnets," *Supercond. Sci. Technol.*, vol. 30, no. 4, Feb. 2017, Art. no. 04LT01.

[15] T. Holubek et al., "A novel concept of high temperature superconducting undulator," *Supercond. Sci. Technol.*, vol. 30, no. 11, Sep. 2017, Art. no. 115002.

[16] A. Will et al., "Design and fabrication concepts of a compact undulator with laser-structured 2G-HTS tapes," in *Proc. 12th Int. Part. Accel. Conf.*, Campinas, SP, Brazil, 2021, pp. 3851–3854.

[17] M. Calvi et al., "GdBCO bulk superconducting helical undulator for x-ray free-electron lasers," *Phys. Rev. Res.*, vol. 5, no. 3, Aug. 2023, Art. no. L032020.

[18] K. Zhang et al., "Record field in a 10 mm-period bulk high-temperature superconducting undulator," *Supercond. Sci. Technol.*, vol. 36, no. 5, Aug. 2023, Art. no. 05LT01.

[19] S. C. Richter et al., "Bending radius limits of different coated REBCO conductor tapes-an experimental investigation with regard to HTS undulators," in *Proc. 12th Int. Part. Accel. Conf.*, 2021, pp. 3837-3840.

[20] "Opera 2020, Simulation Software," 2020. Accessed: Sep. 25, 2023. [Online]. Available: https://www.3ds.com/de/produkte-und-services/simulia/produkte/opera/

[21] S. C. Wimbush and N. M. Strickland, "A public database of high-temperature superconductor critical current data," *IEEE Trans. Appl. Supercond.*, vol. 27, no. 4, Jun. 2017, Art. no. 8000105.

[22] J. Fleiter and A. Ballarino, "Parameterization of the critical surface of REBCO conductors from Fujikura," *Intern. CERN Notes*, Geneva, Switzerland, Rep. no. 2017_31, 2014.

[23] S. C. Richter, "High-temperature superconductor application to undulators for compact free-electron lasers," Ph.D. dissertation, Karlsruhe Inst. Technol. (KIT), Karlsruhe, Germany, Jun. 2023.

[24] "Inc ANSYS. Canonsburg, PA, USA," Ansys 19.1. Accessed: Sep. 25, 2023. [Online]. Available: https://www.ansys.com/

[25] C. Barth, G. Mondonico, and C. Senatore, "Electro-mechanical properties of REBCO coated conductors from various industrial manufacturers at 77K, self-field and 4.2K, 19T," *Supercond. Sci. Technol.*, vol. 28, no. 4, Feb. 2015, Art. no. 045011.

[26] S. Casalbuoni et al., "Performance of a Full Scale Superconducting Undulator with 20 mm Period Length at the KIT Synchrotron," in *Proc. Int. Part. Accel. Conf.*, Vancouver, Canada, 2018, pp. 4223–4225.

[27] J. Fleiter and A. Ballarino, "In-field electrical resistance at 4.2K. of REBCO splices," *IEEE Trans. Appl. Supercond.*, vol. 27, no. 4, Jun. 2017, Art. no. 6603305.

[28] T. H. Nes et al., "Effective time constants at 4.2 to 70K. in REBCO pancake coils with different inter-turn resistances," *IEEE Trans. Appl. Supercond.*, vol. 32, no. 4, Jun. 2022, Art. no. 4600806.